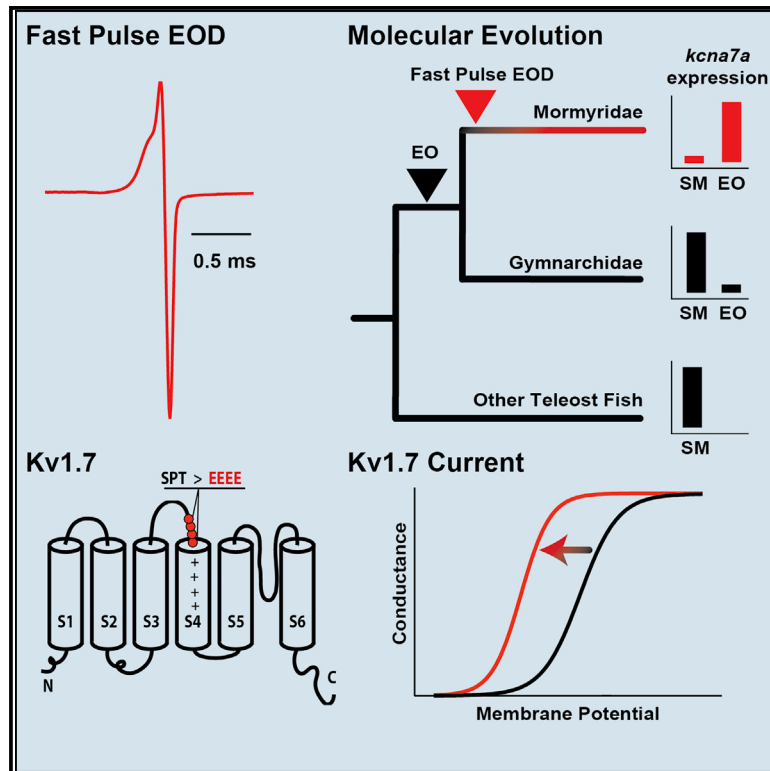


# Current Biology

## Electrostatic Tuning of a Potassium Channel in Electric Fish

### Graphical Abstract



### Authors

Immani Swapna, Alfredo Ghezzi,  
Julia M. York, ..., Ying Lu,  
Jason R. Gallant, Harold H. Zakon

### Correspondence

jgallant@msu.edu (J.R.G.),  
h.zakon@austin.utexas.edu (H.H.Z.)

### In Brief

In electric fish with ultra-brief discharges, Swapna et al. find a potassium channel that shortens action potentials by activating fast and close to resting potential. These properties derive from a patch of negative amino acids near the voltage sensor. Similarly placed charged amino acids may tune voltage sensitivity of channels more generally.

### Highlights

- Some electric fish make brief discharges lasting only a few hundred microseconds
- These fish have evolved a potassium channel that shortens action potentials
- This derives from a patch of negative amino acids above the channel's voltage sensor
- The negative patch adds to surface charge, enhancing sensitivity to depolarization



# Electrostatic Tuning of a Potassium Channel in Electric Fish

Immani Swapna,<sup>1,2</sup> Alfredo Ghezzi,<sup>1,5</sup> Julia M. York,<sup>2</sup> Michael R. Markham,<sup>4</sup> D. Brent Halling,<sup>1</sup> Ying Lu,<sup>1</sup> Jason R. Gallant,<sup>3,\*</sup> and Harold H. Zakon<sup>1,2,6,\*</sup>

<sup>1</sup>Department of Neuroscience, The University of Texas at Austin, Austin, TX 78712, USA

<sup>2</sup>Department of Integrative Biology, The University of Texas at Austin, Austin, TX 78712, USA

<sup>3</sup>Department of Integrative Biology, Michigan State University, East Lansing, MI 48864, USA

<sup>4</sup>Department of Biology, The University of Oklahoma, Norman, OK 73019, USA

<sup>5</sup>Department of Biology, University of Puerto Rico - Rio Piedras, San Juan, PR 00931, USA

<sup>6</sup>Lead Contact

\*Correspondence: [jgallant@msu.edu](mailto:jgallant@msu.edu) (J.R.G.), [h.zakon@austin.utexas.edu](mailto:h.zakon@austin.utexas.edu) (H.H.Z.)

<https://doi.org/10.1016/j.cub.2018.05.012>

## SUMMARY

Molecular variation contributes to the evolution of adaptive phenotypes, though it is often difficult to understand *precisely* how. The adaptively significant electric organ discharge behavior of weakly electric fish is the direct result of biophysical membrane properties set by ion channels. Here, we describe a voltage-gated potassium-channel gene in African electric fishes that is under positive selection and highly expressed in the electric organ. The channel produced by this gene shortens electric organ action potentials by activating quickly and at hyperpolarized membrane potentials. The source of these properties is a derived patch of negatively charged amino acids in an extracellular loop near the voltage sensor. We demonstrate that this negative patch acts by contributing to the global surface charge rather than by local interactions with specific amino acids in the channel's extracellular face. We suggest a more widespread role for this loop in the evolutionary tuning of voltage-dependent channels.

## INTRODUCTION

A major goal of evolutionary biology is understanding how changes at the genetic level result in adaptations. Much can be learned about the genetic basis of adaptation by studying species with unique and/or extreme phenotypic adaptations [1–5]. Because electric fish signal with electricity and those signals are under strong selection and generated by ion channels, electric fish are an excellent system to study how selection may tune ion channels and, especially, how it might push them toward their biophysical limits.

Nocturnally active mormyrid electric fish produce brief, weak-voltage electric fields, called electric organ discharges (EODs), to form electrosensory images of their environments and to communicate during courtship [6]. Though EOD waveforms are known to be influenced by both natural and sexual selection pressures [7–9], the molecular targets and biophysical mecha-

nisms for selection remain elusive. The superfamily Mormyroidea is composed of the Gymnarchidae and the Mormyridae (Figure 1). The family Gymnarchidae is composed of a single species, *Gymnarchus niloticus*, that generates a constant sine wave-like EOD. The sister taxon, the family mormyridae (Figure 1, blue triangle), includes hundreds of species, all of which produce brief, often multi-phasic pulses at variable intervals—“pulse-type” EODs [11].

In the Mormyridae, selection has often favored the evolution of extremely brief EODs [12, 13] and neuronal adaptations to discriminate between timing differences less than 10 microseconds ( $\mu$ s) [14, 15], suggesting that EOD pulse duration must be precisely regulated. EODs are produced by the synchronous discharge of action potentials (APs) from many hundreds of individual electrocytes. These APs are extremely brief ( $\sim$ 200  $\mu$ s) [16, 17]. Because the duration of APs is shaped by potassium currents as well as sodium currents, we assessed whether voltage-gated potassium channels expressed in the mormyrid electric organ (EO) have evolved specializations for generating brief APs. Here, we report a potassium-channel gene with a strong imprint of positive selection that is highly expressed in the EO. The biophysical properties of the channel encoded by this gene are specialized for generating brief APs. These properties result from an evolutionarily novel motif of negatively charged residues in an extracellular loop adjacent to the channel's voltage sensor. The previous understanding of this extracellular loop is largely based on the *shaker* potassium channel in fruit flies. However, our analyses suggest that this loop functions differently in vertebrates and suggests a role for this loop in the evolutionary tuning of ion channels.

## RESULTS

### Identification of a Rapidly Evolving Potassium Channel from Electric Organ

We began by examining muscle and EO transcriptomes representative of *Gymnarchus* and the Mormyridae (Tables S1 and S2; Key Resources Table). We uncovered two orthologs of the mammalian *KCNA7* channel gene—*kcna7a* and *kcna7b*—that duplicated in the teleost whole-genome duplication (Figure S1). In mammals, *KCNA7* is expressed in heart and muscle [18–20]; *kcna7b* is also expressed in muscle in mormyrids (Figure 2).



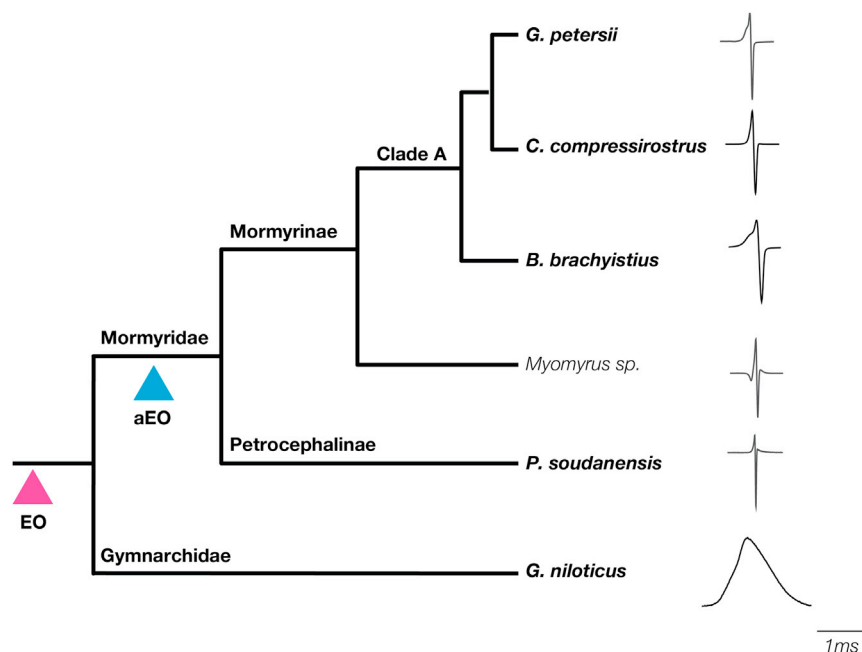


**Figure 1. Major Clades of Mormyroidea with Representative EODs**

Species used in this study are shown in boldface. Electric organs (EO, purple triangle) evolved in the common ancestor of the superfamily mormyroidea that is comprised of two families: the monotypic Gymnarchidae and the Mormyridae. Electric organ discharges (EODs) in *Gymnarchus niloticus* are quasi-sinusoidal wave-like discharges, although only a single cycle is shown here. In the common ancestor of the Mormyridae, a more specialized adult electric organ (aEO, blue triangle) evolved, which produces short-duration pulse-type discharges. EODs of Petrocephalinae (e.g., *Petrocephalus soudanensis*) and non-clade-A mormyriinae (e.g., *Myomyrus* spp.) are characteristically short duration, whereas clade-A mormyriinae are highly diverse in EOD properties, including duration and number of phases (complexity). Some EOD recordings shown derive from specimens deposited in the Cornell Museum of Vertebrates and EOD recordings deposited in the Macaulay Library at the Cornell Laboratory of Ornithology: *Myomyrus macrops* (CUMV 92394; ML EOD 515280), *Brienomyrus brachyistius* (CUMV 80464; ML EOD 510794), *Gnathonemus petersii* (CUMV 87880; ML EOD 510874). EOD

from *Petrocephalus soudanensis* was provided by C.D. Hopkins (Cornell University), and EODs from *Gymnarchus niloticus* and *Campylomormyrus compressirostris* were recorded by J. Gallant from captive laboratory specimens. For details on recording methods see [10].

While *kcna7a* is expressed in muscle in *Gymnarchus*, it is predominantly expressed in the EO in mormyrids where it is virtually the only (~10- to 100-fold higher than any other) voltage-gated potassium-channel gene expressed (Figures 2 and 3B) and

without a beta subunit. The change in expression from muscle to EO in the ancestral mormyrid was accompanied by a burst of positive selection (HYPHY, REL branch-site model [21]) ( $p < 0.01$ , corrected  $p$  value) on this branch (Figures 3A, 3C, and

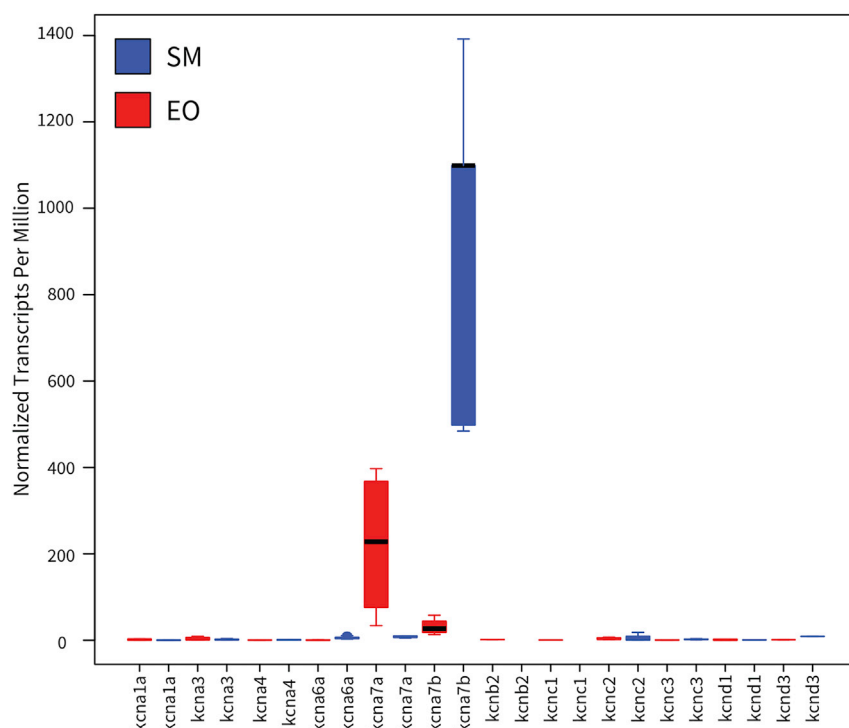


**Figure 2. Box-and-Whisker Plots Showing Relative Expression of Potassium-Channel Genes in Electric Organ and Skeletal Muscle of *Brienomyrus brachyistius***

Many potassium-channel genes were undetectable in the EO; this graph displays only those that were detectable. Note that *Kcna7a* is the predominantly expressed potassium channel in the EO and that *Kcna7b* is the predominantly expressed potassium channel in skeletal muscle. Accession numbers for all potassium channels utilized in this figure are listed in Table S5. See also Tables S1 and S2.

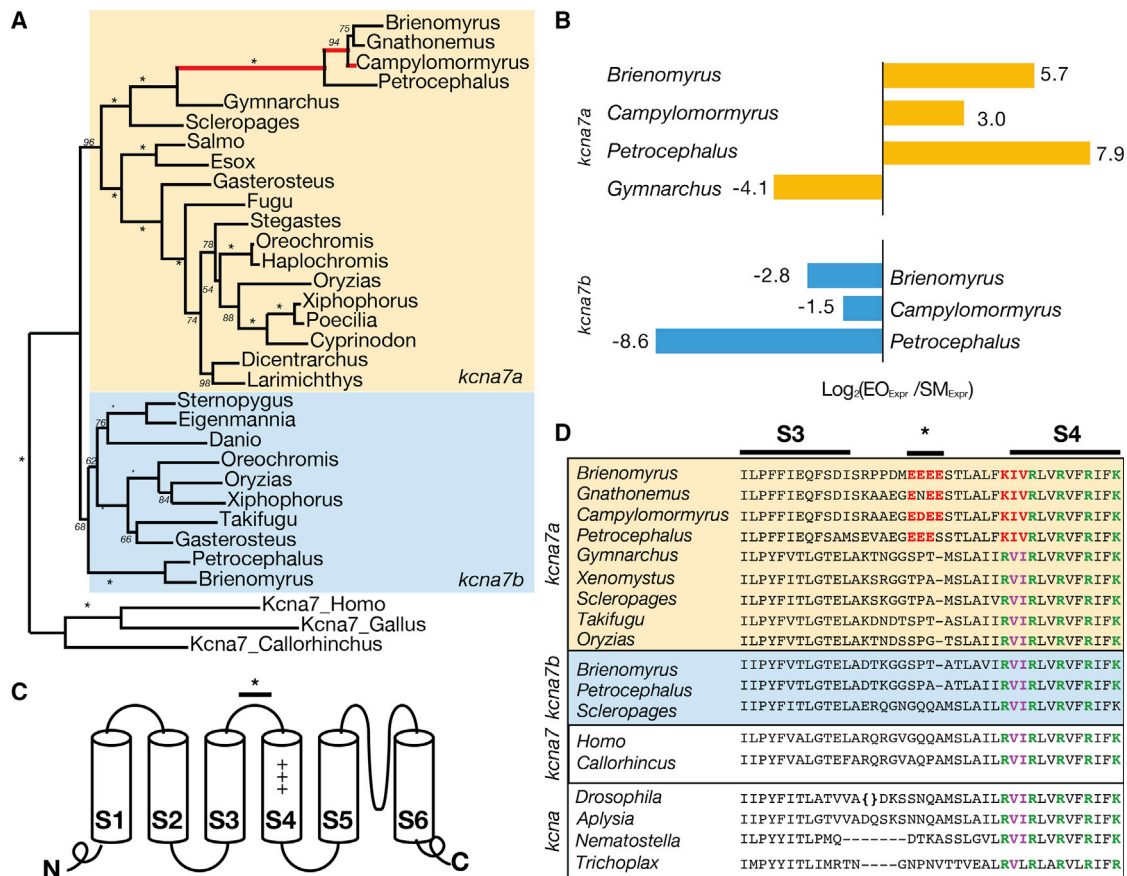


**Figure 3. Evolutionary Change in Electric-Organ-Expressing Potassium Channels of Mormyrid Electric Fish**

(A) Maximum-likelihood gene tree for *kcna7a* and *kcna7b* illustrates the duplication of *KCNA7* in teleosts (asterisks, bootstrap values of 100). Branches displaying episodic diversifying selection are in red ( $p < 0.01$ , corrected  $p$  value). *Petrocephalus* is a basal group, and the other three species are in the derived clade A, giving good phylogenetic coverage of the mormyrids. Note that the burst of episodic selection at the base of pulse-generating mormyrids and within clade A.

(B) Relative expression of *kcna7a* and *kcna7b* in the skeletal muscle (SM) and electric organ (EO) of mormyrids and *Gymnarchus*.

(C) Schematic illustration of potassium channel. Note the voltage sensor (S4) and the S3–S4 linker. A bar represents the portion of the S3–S4 linker that is the focus of our study. The asterisk over the bar indicates the location of a site determined to be under positive selection by HYPHY. The amino acid sequences of this region are shown in (D).

(D) S3–S4 linker and S4 in *shaker* channels (corresponding to amino acids 293–333 of the *Brienomyrus* sequence): *kcna7a* of four mormyrids (*Brienomyrus*, *Gnathonemus*, *Campylomormyrus*, *Petrocephalus*), *Gymnarchus*, and other teleosts (*Xenomystus*, *Scleropages*, *Fugu*, *Oryzias*); *kcna7b* of mormyrids and another teleost and *KCNA7* in human (*Homo*) and elephant shark (*Callorhinchus*); the single *shaker* channel in fruit fly (*Drosophila*) and sea slug (*Aplysia*); and one of six *shaker* channels in sea anemone (*Nematostella*). Conserved positively charged amino acids in S4 in green; conserved hydrophobic amino acids in S4 in violet. Amino acid substitutions in S4 and the S3–S4 linker in mormyrids in red. The S3–S4 linker of the *Drosophila shaker* gene is longer than in vertebrates and is truncated to fit the alignment (parentheses).

See also Figures S1 and S5 and Table S5.

3D), paralleling similar changes in the voltage-gated sodium channel gene, *scn4aa* [22].

### Voltage-Clamp Analysis Shows Biophysical Specializations for Generating Brief Action Potentials

A potassium current can shorten APs if it activates quickly or at a relatively hyperpolarized membrane potential, or if it has a steep conductance-voltage curve. In *Xenopus* oocytes, we expressed both *kcna7a* sequence from *Gymnarchus niloticus*, which expresses *kcna7a* in muscle, and *kcna7a* sequence from *Brienomyrus brachyistius*, a mormyrid that expresses *kcna7a* in EO and has a brief EOD pulse. We observed that the potassium cur-

rent from *Brienomyrus* activates faster ( $\tau$ : *Brienomyrus* =  $1.2 \pm 0.2$  ms; *Gymnarchus* =  $3.0 \pm 1.0$  ms;  $p < 0.0001$ ; Figures 4A, 4C, and 4E), at  $\sim 30$  millivolts (mV) more hyperpolarized membrane potentials ( $V_{1/2}$ : *Brienomyrus* =  $-44.4 \pm 5.7$  mV; *Gymnarchus* =  $-13.1 \pm 5.9$  mV;  $p < 0.0001$ ; Figures 4B and 4D), and with a steeper conductance-voltage (G-V) curve ( $k$ : *Brienomyrus* =  $7.0 \pm 1.4$ ; *Gymnarchus* =  $9.3 \pm 2.3$ ;  $p < 0.028$ ; Figure 4F) than the current from *Gymnarchus*. *Brienomyrus kcna7a* current begins to activate approximately 10–20 mV above electrocyte resting potential ( $-90$  to  $-95$  mV; from [16, 17]). A computational model of electrocyte APs using the parameters from these recordings together with generic sodium currents and an inward

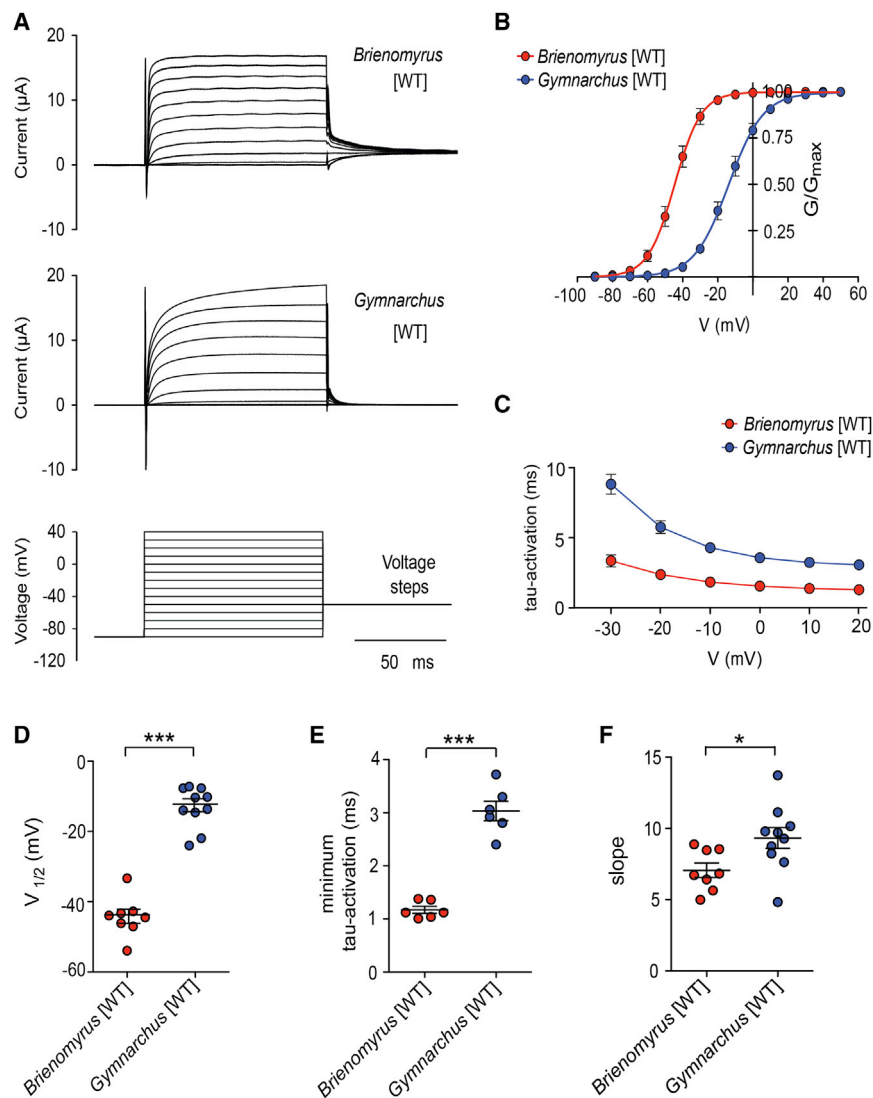


**Figure 4. Currents from *kcna7a* of *Gymnarchus* and *Brienomyrus* Expressed in *Xenopus* Oocytes Show Striking Differences**

(A–F) Raw voltage-clamp traces (A), conductance-voltage (G–V) curves (B), time constant of activation ( $\tau$ ) as a function of voltage (C), the voltage at which the conductance is 50% of maximum ( $V_{1/2}$ ) (D), minimum  $\tau$  (taken at +20 mV) (E), and the slope of the G–V curve (F). Note that the expressed current from *Brienomyrus* activates faster, at more hyperpolarized voltages, and with a steeper slope than that from *Gymnarchus*. Here and in all subsequent figures, *Gymnarchus*, blue; *Brienomyrus*, red. \* $p < 0.05$ , \*\*\* $p < 0.001$  (unpaired  $t$  test). Here and in subsequent figures, the brief downward deflection at the onset of the voltage clamp is caused by ringing as the clamp settles. See also Figure S2 and Tables S3, S4, and S7.

form a channel. S5 and S6 line a conductive pore for potassium that opens when membrane depolarization alters the conformations of S4, which forms the voltage sensor. The *kcna7a* gene, which encodes the Kv1.7a potassium-channel protein, is a member of the *shaker* family of potassium channels named after the canonical *shaker* gene of *Drosophila*. The *shaker* family is ancient, preceding the divergence of bilateria and cnidaria [23]. We constructed alignments of Kv1.7 channel proteins with their orthologs, including distantly related *shaker* family channels (Figure 3D). These protein alignments highlight that, despite strong conservation of the amino acids in the S4 over ~800 million years [24], three amino acid substitutions occurred in the S4 of

the ancestor of the pulse mormyrids following the mormyrids' divergence from *Gymnarchus* and before their radiation [25] (Figure 3D).

rectifier found that the current generated by the *Brienomyrus kcna7a* sequence shortens modeled action potential durations more than that of *Gymnarchus* (Figure S2). If *Brienomyrus kcna7a* is adapted for generating brief APs, then *kcna7a* from another pulse-type mormyrid should show similar enhanced voltage sensitivity. Conversely, if *Gymnarchus kcna7a* represents the “default” condition associated with muscle function, then it should have a comparable voltage sensitivity to other muscle-expressing *kcna7* channels. Indeed, the voltage sensitivity of the EO-expressing *kcna7a* from another mormyrid with a brief EOD pulse, *Campylomorus compressirostris* ( $-52.8 \pm 1.8$  mV), is comparable to the EO-expressing *kcna7a* of *Brienomyrus*, and that of the muscle-expressing *Brienomyrus kcna7b* ( $-24.7 \pm 1.3$  mV) and mouse *kcna7* ( $V_{1/2} = -20$  mV) [19] are comparable to *Gymnarchus kcna7a* (Table S7).

#### Site-Directed Mutagenesis Identifies a Novel Functional Motif

Potassium channels have six transmembrane helices, S1–S6, in the alpha subunit (Figure 3C). Four alpha subunits combine to

the ancestor of the pulse mormyrids following the mormyrids' divergence from *Gymnarchus* and before their radiation [25] (Figure 3D).

We tested whether these amino acid substitutions alter channel properties by swapping amino acid residues reciprocally between the *Gymnarchus* and *Brienomyrus* Kv1.7a proteins using site-directed mutagenesis. Placing the three amino acids from the S4 of *Brienomyrus* (Figures S3A–S3C; Table S7) into the S4 of *Gymnarchus* [RVI>KIV] produced a modest shift in the expected direction (leftward) of the G–V curve and complex shifts in activation kinetics, suggesting that amino acids at other sites interact with these to influence tau-activation (Figures S3D and S3E; Table S7). The complementary substitutions from *Gymnarchus* to *Brienomyrus* [KIV>RVI] had no effect on voltage sensitivity and only minor effects on tau-activation (Figure S4; Table S7). Especially considering the last result, we concluded that other amino acid substitutions accrued during the evolution of the ancestral pulse mormyrid Kv1.7a and that the effects of these substitutions must override the effects of the substitutions in S4.

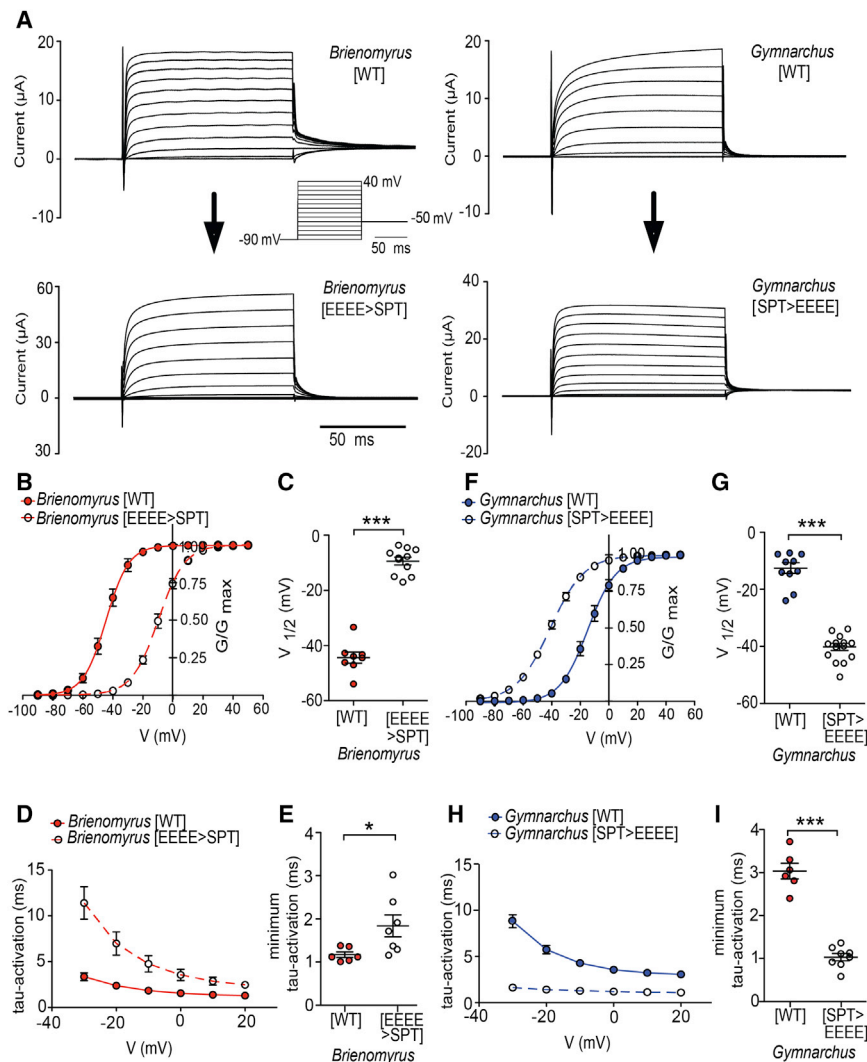


**Figure 5. The Distinctive Characteristics of the Currents from *Kcna7a* of *Gymnarchus* and *Brienomyrus* Are Transferred by Swapping Part of the S3–S4 Linker**

(A–E) Currents of *Brienomyrus* wild-type (WT) and *Brienomyrus* (EEEE>SPT). Raw currents (A), G–V curves (B),  $V_{1/2}$  (C), tau-activation (D), and minimum tau-activation (E).

(F–I) Currents of *Gymnarchus* WT and *Gymnarchus* (SPT>EEEE). G–V curves (F),  $V_{1/2}$  (G), tau-activation (H), and minimum tau-activation (I). Here and in all subsequent figures, solid lines, WT; dotted lines, chimeric channels. \* $p < 0.05$ , \*\*\* $p < 0.001$  (unpaired  $t$  test).

See also Figures S3 and S4 and Tables S6 and S7.

differing by only one amino acid (Figure 3D). However, we note that the S3–S4 linker of the *shaker* channel of *Drosophila* and other arthropods is atypically long compared with that of other animals (Figures 3 and S5), suggesting that the S3–S4 linker may function differently in arthropods than in other animals. Therefore, we made a structural model of the Kv1.7a S3–S4 linkers of *Brienomyrus* and *Gymnarchus*.

The extra negative charges in the S3–S4 linker of *Brienomyrus* could contribute to different physical properties between the channels of the two species, including flexibility and charge. We compared the S3–S4 linkers of homology models of the *Gymnarchus* and the *Brienomyrus* Kcna7a voltage sensors (Figure S6). Taken as a whole, the overall content of flexible voltage-sensor residues is comparable, emphasizing that the differences

between S3–S4 linkers that transfer with the “negative patch” is likely not due to flexibility.

### Electrostatic Tuning of the Voltage Sensor

To test whether the additional glutamates act *via* their electrostatic properties, we conducted two experiments: replacing negatively charged aspartates for glutamates did not alter  $V_{1/2}$  ( $V_{1/2}$  [EEEE>DDDD] =  $-49.2 \pm 4.9$  mV), and replacement with positively charged amino acids produced an even more profound rightward shift of voltage sensitivity than replacement with *Gymnarchus*’ neutral amino acids ( $V_{1/2}$  [EEEE>KKKK] =  $+16.0 \pm 9.2$  mV; ns  $p > 0.05$ , \*\*\* $p < 0.001$ ; one-way ANOVA followed by Dunnett’s post-test) (Figure 6; Table S7).

How might the negative patch influence channel behavior? The “repulsion hypothesis” suggests that this patch might face another negatively charged amino acid or patch of amino acids in the closed state. Under these conditions, a focused, local interaction between the two could create a repulsive bias so that less depolarizing voltage is needed to move the S4 [31]. Alternatively, the negatively charged amino acids in this region may be forming salt bridges with positively charged amino acids in other parts

The mormyrid kv1.7a is unusual among vertebrate voltage-gated potassium channels at another place: it possesses a patch of contiguous negatively charged amino acids in the S3–S4 linker (Figure 3D). A site within this patch was detected by HYPHY as evolving under positive selection (Figures 3C and 3D, asterisk). Again, using site-directed mutagenesis, we swapped homologous regions of the S3–S4 linker between *Gymnarchus* and *Brienomyrus* channels. This resulted in a strong shift in the  $V_{1/2}$  and tau-activation of one species to that of the other (*Brienomyrus* [EEEE>SPT] =  $-9.3 \pm 4.6$  mV; *Gymnarchus* [SPT>EEEE] =  $-40.7 \pm 4.7$  mV) (wild-type [WT] versus chimeric channel in both species,  $p < 0.0001$ ) (Figure 5; Table S7).

### Predicted Structural Properties of S3–S4 Linkers

There is an increasing recognition that the S3–S4 linker influences potassium-channel properties [26]. The prevailing view is that the S3–S4 linker’s influence on *Drosophila shaker* channel properties is due to its length and flexibility rather than its charged residues [27–30]. We note that the S3–S4 linkers in *Brienomyrus* and *Gymnarchus Kcna7a* are almost identical in length,

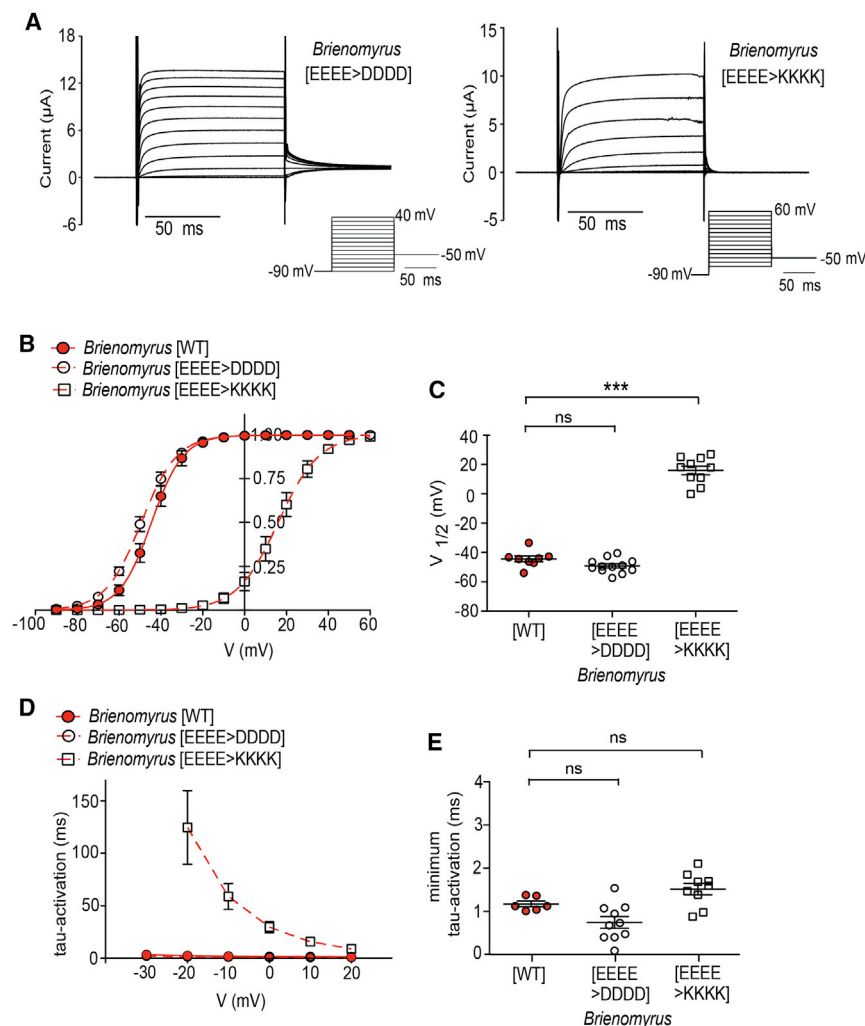


**Figure 6. Substitution of Negatively Charged (D) but Not Positively Charged (K) Amino Acids in the Brienyomys S3-S4 Linker Retains WT Biophysical Properties**

(A–E) Representative currents (A), conductance-voltage curves (B),  $V_{1/2}$  values (C), tau-activation curves (D), and minimum tau-activation curves (E). Insets below traces in (A) are the voltage protocols used and the statistics information. ns, not significant ( $p \geq 0.05$ ); \*\*\* $p < 0.001$  (one-way ANOVA followed by the Dunnett's posttest) compared to WT. See also Figures S5 and S6 and Table S7.

the S3–S4 linker is not acting *via* a local repulsive force or formation of salt bridges but rather globally by contributing to the surface charge.

## DISCUSSION

At the origin of the mormyrids, *kcna7a* shifted its expression from its ancestral location in skeletal muscle to strong selectivity for expression in the EO, where it is the vastly predominant potassium channel in the EO. Accompanying this shift in expression, the *kcna7a* potassium-channel gene evolved rapidly, preceding the adaptive radiation of the mormyrids. This is a similar pattern to that of a muscle-expressing sodium-channel gene that also shifted its expression to the mormyrid EO (*scn4aa*) [22, 32]. Because of (1) the near exclusive expression of *kcna7a* over other voltage-gated potassium channels in the EO, (2) the observed amino acid substitu-

tions in the S3–S4 linker in Kv1.7a, and (3) our measurements of the biophysical properties of the mormyrid channel compared to its ancestral form, we conclude that these biophysical changes enable ultra-brief EODs by shortening the duration of APs produced by electrocytes. Ultimately, this conclusion must be tested by recording native currents of electrocytes. While there are a number of other amino acid substitutions at conserved sites, future studies will elucidate their functions. We note that a few species of mormyrids, such as *Campylomormyris tshokwe*, have secondarily and independently evolved long-duration EOD pulses [8, 33, 34]. The expression level of some Kv1 family genes [35] have been implicated in species differences in EOD duration in the explosively radiating genus *Campylomormyris*, though *kcna7a* paralogs have not been examined in this group. It will be interesting to examine whether additional novel amino acid substitutions have occurred in *C. tshokwe kcna7a* and within other species with long-duration EOD pulses.

of the channel favoring the open confirmation. The “surface charge” hypothesis states that the charged intra- and extracellular parts of proteins globally add to, or cancel out, the membrane potential caused by separation of ions. In this way, S4 movement could occur at less depolarized membrane potentials. To distinguish between these hypotheses, we devised a test based on the premise that if a local bias occurs *via* a local electrostatic repulsion, it should not matter if interacting partners are negative or positive. We identified negatively charged putative interaction partners primarily in extracellular loops near the S3–S4 linker (S3–S4, S1–S2) or in the S5-pore that were conceivably close enough to have an electrostatic interaction with the S3–S4 linker, converted them to positive residues (E/D>K), and tested whether this altered  $V_{1/2}$  (Figure 7). Some substitutions had little effect, but some, such as D379K, made  $V_{1/2}$  more positive. We then combined any substitutions that shifted  $V_{1/2}$  with the positively charged [EEEE>KKKK] S3–S4 linker. We observed that the combination of two positive patches only shifted  $V_{1/2}$  to even more positive values, never a reversion to a more negative  $V_{1/2}$ . Substituting the positive amino acids in the extracellular loop regions to negative amino acids did not have any effect on the  $V_{1/2}$ . These results suggest that the negative patch in

the prevailing view of the S3–S4 linker's influence on *shaker* channel properties is that it is due to its length, flexibility, or hydrophobicity rather than its charged residues [27–30]. Our data show that the long S3–S4 linker of the *Drosophila shaker* and other arthropods is not representative of other animal groups,

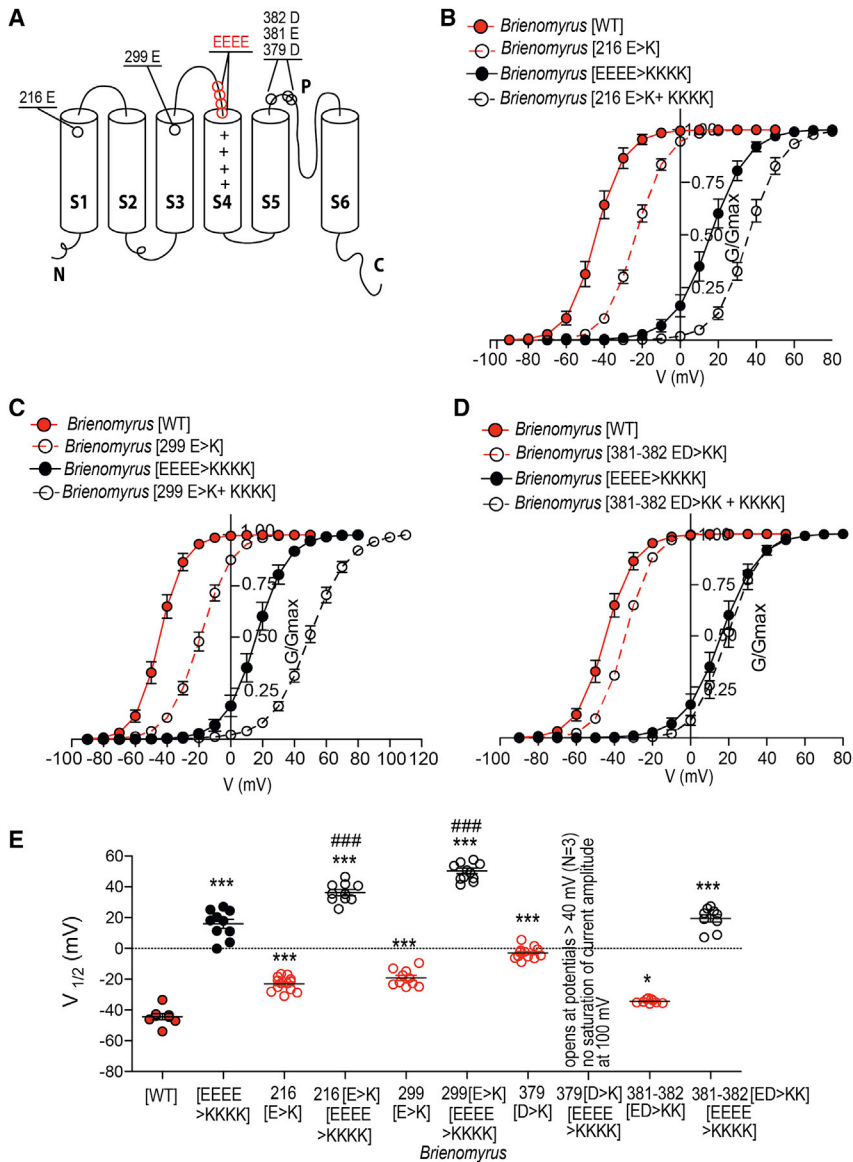


**Figure 7. Expression of Paired Amino Acid Substitutions Suggests that the S3-S4 Linker Negative Patch Acts via Surface Charge**

Summary showing negatively charged amino acids (E, D) in S1-S2, S3-S4, and S5-S6 loops that had quantitatively measurable effect on V<sub>1/2</sub> when substituted with the positively charged amino acid lysine (K), alone and in combination with S3-S4 EEEE>K K K K K in *Brienomyrus* kv1.7a.

(A) Schematic diagram of site of amino acid substitutions in S1-S2, S3-S4, S5-S6 (black), and S3-S4 (red) that caused a significant measurable shift in V<sub>1/2</sub>.

(B-D) G-V curves for amino acid substitutions in S1-S2 loop (B), S3-S4 loop (C), and S5-S6 loop (D) that affected V<sub>1/2</sub> in combination with S3-S4 EEEE>K K K K K substitutions.

(E) Summary of V<sub>1/2</sub> for all groups depicted in this figure. For information on all substitutions made in the S1-S2, S3-S4, and S5-S6 loops to assess possible electrostatic interactions with the S3-S4 loop EEEE region in *Brienomyrus* kv1.7a, see Table S7.

\* indicates significance (\*p < 0.05, \*\*\*p < 0.001) compared to *Brienomyrus* kv1.7a (WT) calculated using one-way ANOVA followed by Dunnett's posttest. # indicates significance (###p < 0.001) compared to *Brienomyrus* kv1.7a [EEEE>K K K K K] calculated using one-way ANOVA followed by Dunnett's posttest. See also Figure S6.

including vertebrates (Figure S5). The S3-S4 linker of mormyrids possesses a naturally occurring, extreme but instructive case of a large patch of negatively charged amino acids poised directly above the S4; other vertebrate potassium channels have negatively charged amino acids at one or more sites within the S3-S4 linker that could mediate such effects. Our study and a few other recent studies [31, 36] suggest that negative charges acting to alter outer-membrane surface charge rather than flexibility are at play in tuning the voltage sensitivity of vertebrate voltage-gated potassium channels. This concept is further supported by a complementary observation of an L-type Ca<sup>2+</sup> channel found in elasmobranch electroreceptors that activates at more hyperpolarized potentials than expected due to a patch of positively charged amino acids in the S2-S3 linker localized near the inner mouth of the channel [37]. Thus, it seems that the addition of charged amino acids on either side of the S4 voltage sensor may be an evolutionarily simple and widespread way to modify channel voltage sensitivity and gating kinetics.

## STAR★METHODS

Detailed methods are provided in the online version of this paper and include the following:

- KEY RESOURCES TABLE
- CONTACT FOR REAGENT AND RESOURCE SHARING
- EXPERIMENTAL MODEL AND SUBJECT DETAILS
  - Animal Sources
  - Oocytes
- METHOD DETAILS
  - RNA Extraction and Library Preparation for RNAseq
  - Additional Data Sources
  - Transcriptome Assembly
  - Calculation of Expression Levels
  - Assignment of Orthologues Between Electric Fish
  - Mutagenesis and Expression in Oocytes
  - Electrophysiology and Analysis

- Computational Methods and Results
- Structure Models
- **QUANTIFICATION AND STATISTICAL ANALYSIS**
  - Phylogenetic Analysis
  - Electrophysiology
- **DATA AND SOFTWARE AVAILABILITY**

#### SUPPLEMENTAL INFORMATION

Supplemental Information includes six figures and seven tables and can be found with this article online at <https://doi.org/10.1016/j.cub.2018.05.012>.

#### ACKNOWLEDGEMENTS

The sequence data reported here are available from NCBI (accession numbers given in supplementary materials). Funding for this work was by NSF IOS# 1557657 (J.R.G.), NSF IOS# 1557857 (H.H.Z.), NSF IOS# 1350753 and IOS# 1257580 (M.R.M.), and NIH 2R01NS077821 to Richard Aldrich.

#### AUTHOR CONTRIBUTIONS

Conceptualization, H.H.Z. and J.R.G.; Methodology, H.H.Z., I.S., and J.R.G.; Investigation, I.S., A.G., H.H.Z., J.R.G., M.R.M., D.B.H., Y.L., and J.M.Y.; Writing – Original Draft, H.H.Z. and J.R.G.; Writing – Review & Editing, H.H.Z., J.R.G., I.S., M.R.M., and D.B.H.; Funding Acquisition, H.H.Z., M.R.M., and J.R.G.; Supervision, H.H.Z. and J.R.G.

#### DECLARATION OF INTERESTS

The authors declare no competing interests.

Received: December 6, 2017

Revised: April 3, 2018

Accepted: May 3, 2018

Published: June 21, 2018

#### REFERENCES

1. Gallant, J.R., Traeger, L.L., Volkening, J.D., Moffett, H., Chen, P.H., Novina, C.D., Phillips, G.N., Jr., Anand, R., Wells, G.B., Pinch, M., et al. (2014). Nonhuman genetics. Genomic basis for the convergent evolution of electric organs. *Science* *344*, 1522–1525.
2. Gracheva, E.O., Cordero-Morales, J.F., González-Carcacia, J.A., Ingolia, N.T., Manno, C., Aranguren, C.I., Weissman, J.S., and Julius, D. (2011). Ganglion-specific splicing of TRPV1 underlies infrared sensation in vampire bats. *Nature* *476*, 88–91.
3. Gracheva, E.O., Ingolia, N.T., Kelly, Y.M., Cordero-Morales, J.F., Hollopeter, G., Chesler, A.T., Sánchez, E.E., Perez, J.C., Weissman, J.S., and Julius, D. (2010). Molecular basis of infrared detection by snakes. *Nature* *464*, 1006–1011.
4. Rowe, A.H., Xiao, Y., Rowe, M.P., Cummins, T.R., and Zakon, H.H. (2013). Voltage-gated sodium channel in grasshopper mice defends against bark scorpion toxin. *Science* *342*, 441–446.
5. Tarvin, R.D., Borghese, C.M., Sachs, W., Santos, J.C., Lu, Y., O’Connell, L.A., Cannatella, D.C., Harris, R.A., and Zakon, H.H. (2017). Interacting amino acid replacements allow poison frogs to evolve epibatidine resistance. *Science* *357*, 1261–1266.
6. Dunlap, K., Silva, A., Smith, G., and Zakon, H. (2017). Weakly electric fish: Behavior, neurobiology and neuroendocrinology. In *Hormones, Brain and Behavior, Third Edition*, B. Hormones, D.P. Behavior, and M. Joels, eds. (Oxford: Academic Press), pp. 69–98.
7. Hopkins, C.D. (1973). Lightning as background noise for communication among electric fish. *Nature* *424*, 268–270.
8. Hopkins, C.D. (1981). On the diversity of electric signals in a community of mormyrid electric fish in West Africa. *Am. Zool.* *21*, 211–222.
9. Stoddard, P.K. (1999). Predation enhances complexity in the evolution of electric fish signals. *Nature* *400*, 254–256.
10. Gallant, J.R., Arnegard, M.E., Sullivan, J.P., Carlson, B.A., and Hopkins, C.D. (2011). Signal variation and its morphological correlates in *Paramormyrops kingsleyae* provide insight into the evolution of electrogenic signal diversity in mormyrid electric fish. *J. Comp. Physiol. A Neuroethol. Sens. Neural Behav. Physiol.* *197*, 799–817.
11. Carlson, B.A., Hasan, S.M., Hollmann, M., Miller, D.B., Harmon, L.J., and Arnegard, M.E. (2011). Brain evolution triggers increased diversification of electric fishes. *Science* *332*, 583–586.
12. Hopkins, C.D. (1980). Evolution of electric communication channels of mormyrids. *Behav. Ecol. Sociobiol.* *7*, 1–13.
13. von der Emde, G., and Ringer, T. (1992). Electrolocation of Capacitive Objects in Four Species of Pulse-type Weakly Electric Fish I. Discrimination Performance. *Ethology* *91*, 326–338.
14. Hopkins, C.D., and Bass, A.H. (1981). Temporal coding of species recognition signals in an electric fish. *Science* *212*, 85–87.
15. Paintner, S., and Kramer, B. (2003). Electrosensory basis for individual recognition in a weakly electric, mormyrid fish, *Pollimyrus adspersus* (Günther, 1866). *Behav. Ecol. Sociobiol.* *55*, 197–208.
16. Bass, A.H., and Volman, S.F. (1987). From behavior to membranes: testosterone-induced changes in action potential duration in electric organs. *Proc. Natl. Acad. Sci. USA* *84*, 9295–9298.
17. Bennett, M.V.L. (1971). Electric organs. In *Fish physiology, Volume 5*, D.J. Randall, ed. (New York: Academic Press), pp. 347–491.
18. Finol-Urdaneta, R.K., Strüver, N., and Terlau, H. (2006). Molecular and functional differences between heart mKv1.7 channel isoforms. *J. Gen. Physiol.* *128*, 133–145.
19. Kalman, K., Nguyen, A., Tseng-Crank, J., Dukes, I.D., Chandy, G., Hustad, C.M., Copeland, N.G., Jenkins, N.A., Mohrenweiser, H., Brandriff, B., et al. (1998). Genomic organization, chromosomal localization, tissue distribution, and biophysical characterization of a novel mammalian Shaker-related voltage-gated potassium channel, Kv1.7. *J. Biol. Chem.* *273*, 5851–5857.
20. Kashuba, V.I., Kvasha, S.M., Protodopov, A.I., Gizatullin, R.Z., Rynditch, A.V., Wahlestedt, C., Wasserman, W.W., and Zabarovsky, E.R. (2001). Initial isolation and analysis of the human Kv1.7 (KCNA7) gene, a member of the voltage-gated potassium channel gene family. *Gene* *268*, 115–122.
21. Pond, S.L.K., Frost, S.D.W., and Muse, S.V. (2005). HyPhy: hypothesis testing using phylogenies. *Bioinformatics* *21*, 676–679.
22. Arnegard, M.E., Zwickl, D.J., Lu, Y., and Zakon, H.H. (2010). Old gene duplication facilitates origin and diversification of an innovative communication system—twice. *Proc. Natl. Acad. Sci. USA* *107*, 22172–22177.
23. Jegla, T., Marlow, H.Q., Chen, B., Simmons, D.K., Jacobo, S.M., and Martindale, M.Q. (2012). Expanded functional diversity of shaker K<sup>+</sup> channels in cnidarians is driven by gene expansion. *PLoS ONE* *7*, e51366.
24. Erwin, D.H. (2015). Early metazoan life: divergence, environment and ecology. *Philos. Trans. R. Soc. Lond. B Biol. Sci.* *370*, 20150036.
25. Lavoué, S., Miya, M., Arnegard, M.E., Sullivan, J.P., Hopkins, C.D., and Nishida, M. (2012). Comparable ages for the independent origins of electrogenesis in African and South American weakly electric fishes. *PLoS ONE* *7*, e36287.
26. Labro, A.J., Priest, M.F., Lacroix, J.J., Snyders, D.J., and Bezanilla, F. (2015). Kv3.1 uses a timely resurgent K(+) current to secure action potential repolarization. *Nat. Commun.* *6*, 10173.
27. Carvalho-de-Souza, J.L., and Bezanilla, F. (2018). Nonsensing residues in S3–S4 linker’s C terminus affect the voltage sensor set point in K<sup>+</sup> channels. *J. Gen. Physiol.* *150*, 307–321.
28. Gonzalez, C., Rosenman, E., Bezanilla, F., Alvarez, O., and Latorre, R. (2000). Modulation of the Shaker K(+) channel gating kinetics by the S3–S4 linker. *J. Gen. Physiol.* *115*, 193–208.
29. Mathur, R., Zheng, J., Yan, Y., and Sigworth, F.J. (1997). Role of the S3–S4 linker in Shaker potassium channel activation. *J. Gen. Physiol.* *109*, 191–199.

30. Priest, M.F., Lacroix, J.J., Villalba-Galea, C.A., and Bezanilla, F. (2013). S3-S4 linker length modulates the relaxed state of a voltage-gated potassium channel. *Biophys. J.* *105*, 2312–2322.
31. Sand, R., Sharmin, N., Morgan, C., and Gallin, W.J. (2013). Fine-tuning of voltage sensitivity of the Kv1.2 potassium channel by inter-helix loop dynamics. *J Biol Chem* *288*, 9686–9695.
32. Paul, C., Kirschbaum, F., Mamonekene, V., and Tiedemann, R. (2016). Evidence for non-neutral evolution in a sodium channel gene in African weakly electric fish (*Campylomormyrus*, Mormyridae). *J. Mol. Evol.* *83*, 61–77.
33. Lamanna, F., Kirschbaum, F., Waurick, I., Dieterich, C., and Tiedemann, R. (2015). Cross-tissue and cross-species analysis of gene expression in skeletal muscle and electric organ of African weakly-electric fish (Teleostei; Mormyridae). *BMC Genomics* *16*, 668.
34. Sullivan, J.P., Lavoué, S., and Hopkins, C.D. (2002). Discovery and phylogenetic analysis of a riverine species flock of African electric fishes (Mormyridae: Teleostei). *Evolution* *56*, 597–616.
35. Nagel, R., Kirschbaum, F., and Tiedemann, R. (2017). Electric organ discharge diversification in mormyrid weakly electric fish is associated with differential expression of voltage-gated ion channel genes. *J. Comp. Physiol. A Neuroethol. Sens. Neural Behav. Physiol.* *203*, 183–195.
36. Elinder, F., Madeja, M., Zeberg, H., and Århem, P. (2016). Extracellular linkers completely transplant the voltage dependence from Kv1.2 ion channels to Kv2.1. *Biophys. J.* *111*, 1679–1691.
37. Bellono, N.W., Leitch, D.B., and Julius, D. (2017). Molecular basis of ancestral vertebrate electroreception. *Nature* *543*, 391–396.
38. Liman, E.R., Tytgat, J., and Hess, P. (1992). Subunit stoichiometry of a mammalian K<sup>+</sup> channel determined by construction of multimeric cDNAs. *Neuron* *9*, 861–871.
39. Bolger, A.M., Lohse, M., and Usadel, B. (2014). Trimmomatic: a flexible trimmer for Illumina sequence data. *Bioinformatics* *30*, 2114–2120.
40. Grabherr, M.G., Haas, B.J., Yassour, M., Levin, J.Z., Thompson, D.A., Amit, I., Adiconis, X., Fan, L., Raychowdhury, R., Zeng, Q., et al. (2011). Full-length transcriptome assembly from RNA-Seq data without a reference genome. *Nat. Biotechnol.* *29*, 644–652.
41. Langmead, B., Trapnell, C., Pop, M., and Salzberg, S.L. (2009). Ultrafast and memory-efficient alignment of short DNA sequences to the human genome. *Genome Biol.* *10*, R25.
42. Li, B., and Dewey, C.N. (2011). RSEM: accurate transcript quantification from RNA-Seq data with or without a reference genome. *BMC Bioinformatics* *12*, 323.
43. Haas, J., Roth, S., Arnold, K., Kiefer, F., Schmidt, T., Bordoli, L., and Schwede, T. (2013). The Protein Model Portal—a comprehensive resource for protein structure and model information. *Database (Oxford)* *2013*, bat031.
44. Krieger, E., Joo, K., Lee, J., Lee, J., Raman, S., Thompson, J., Tyka, M., Baker, D., and Karplus, K. (2009). Improving physical realism, stereochemistry, and side-chain accuracy in homology modeling: Four approaches that performed well in CASP8. *Proteins* *77 (Suppl 9)*, 114–122.
45. Baker, N.A., Sept, D., Joseph, S., Holst, M.J., and McCammon, J.A. (2001). Electrostatics of nanosystems: application to microtubules and the ribosome. *Proc. Natl. Acad. Sci. USA* *98*, 10037–10041.
46. Dolinsky, T.J., Nielsen, J.E., McCammon, J.A., and Baker, N.A. (2004). PDB2PQR: an automated pipeline for the setup of Poisson-Boltzmann electrostatics calculations. *Nucleic Acids Res.* *32*, W665–W667.
47. Lamanna, F., Kirschbaum, F., and Tiedemann, R. (2014). De novo assembly and characterization of the skeletal muscle and electric organ transcriptomes of the African weakly electric fish *Campylomormyrus compressirostris* (Mormyridae, Teleostei). *Mol. Ecol. Resour.* *14*, 1222–1230.
48. Robinson, M.D., and Oshlack, A. (2010). A scaling normalization method for differential expression analysis of RNA-seq data. *Genome Biol.* *11*, R25.
49. Kosakovsky Pond, S.L., Murrell, B., Fourment, M., Frost, S.D.W., Delport, W., and Scheffler, K. (2011). A random effects branch-site model for detecting episodic diversifying selection. *Mol. Biol. Evol.* *28*, 3033–3043.
50. Ban, Y., Smith, B.E., and Markham, M.R. (2015). A highly polarized excitable cell separates sodium channels from sodium-activated potassium channels by more than a millimeter. *J. Neurophysiol.* *114*, 520–530.
51. Markham, M.R., Kaczmarek, L.K., and Zakon, H.H. (2013). A sodium-activated potassium channel supports high-frequency firing and reduces energetic costs during rapid modulations of action potential amplitude. *J. Neurophysiol.* *109*, 1713–1723.
52. Markham, M.R., and Zakon, H.H. (2014). Ionic mechanisms of microsecond-scale spike timing in single cells. *J. Neurosci.* *34*, 6668–6678.
53. Bhaskaran, R., and Ponnuswamy, P.K. (1988). Positional flexibilities of amino acid residues in globular proteins. *Int. J. Pept. Protein Res.* *32*, 241–255.

## STAR★METHODS

## KEY RESOURCES TABLE

REAGENT or RESOURCE	SOURCE	IDENTIFIER
Critical Commercial Assays		
QuikChange II XL site-directed Mutagenesis Kit	Agilent Technologies	Cat# 200521
mMESSAGE mMACHINE T7 Transcription Kit	ThermoFisher Scientific	Cat# AM1344
Deposited Data		
<i>B. brachysitius</i> EO and SM RNA Seq Reads	NCBI SRA BioProject	NCBI BioProject: PRJNA248545
<i>C. compressirostrus</i> EO and SM RNA Seq Reads	NCBI SRA BioProject	NCBI BioProject: PRJNA192446
<i>P. soudanensis</i> SM and EO RNA Seq Reads	This Paper	SRP136188
<i>G. niloticus</i> SM and EO RNA Seq Reads	This Paper	SRP136186
Potassium Channel Sequences from Various Species	NCBI / ENSEMBL	See <a href="#">Tables S5</a> and <a href="#">S6</a>
Experimental Models		
<i>Xenopus Leavis</i> (9+ cm Mature Female, pigmented, 2 to 2.5 years age)	Nasco, WI	ITEM# LM00535MX
Recombinant DNA		
pGEMHE Vector	<a href="#">[38]</a>	N/A
<i>B. brachysitius</i> Kcna7a WT cds in pGEMHE with codon optimization for expression in <i>Xenopus Leavis</i>	GenScript, NJ	N/A
<i>G. niloticus</i> Kcna7a WT cds in pGEMHE with codon optimization for expression in <i>Xenopus Leavis</i>	GenScript, NJ	N/A
<i>B. brachysitius</i> Kcna7b WT cds in pGEMHE with codon optimization for expression in <i>Xenopus Leavis</i>	GenScript, NJ	N/A
<i>C. compressirostrus</i> Kcna7a WT cds in pGEMHE with codon optimization for expression in <i>Xenopus Leavis</i>	GenScript, NJ	N/A
<i>B. brachysitius</i> Kcna7a mutations	This Paper	See <a href="#">Table S7</a>
<i>G. niloticus</i> Kcna7a mutations	This Paper	See <a href="#">Table S7</a>
Software and Algorithms		
Trimmomatic v. 0.33	<a href="#">[39]</a>	<a href="http://www.usadellab.org/cms/?page=trimmomatic">http://www.usadellab.org/cms/?page=trimmomatic</a>
Trinity v. 20140413p1	<a href="#">[40]</a>	<a href="http://trinitymaseq.github.io">http://trinitymaseq.github.io</a>
Bowtie 2 v. 2.2.6	<a href="#">[41]</a>	<a href="http://bowtie-bio.sourceforge.net/bowtie2/index.shtml">http://bowtie-bio.sourceforge.net/bowtie2/index.shtml</a>
RSEM v. 1.3.0	<a href="#">[42]</a>	<a href="https://deweylab.github.io/RSEM/">https://deweylab.github.io/RSEM/</a>
Protein Modeling Portal	<a href="#">[43]</a>	<a href="https://www.proteinmodelportal.org">https://www.proteinmodelportal.org</a>
Yasara Server	<a href="#">[44]</a>	<a href="http://www.yasara.org/minimizationserver.htm">http://www.yasara.org/minimizationserver.htm</a>
PyMOL Molecular Graphics System v. 0.99rc6	Schrödinger	<a href="https://pymol.en.uptodown.com/windows">https://pymol.en.uptodown.com/windows</a>
PDP2PQR	<a href="#">[45]</a>	<a href="https://sourceforge.net/projects/pdb2pqr/">https://sourceforge.net/projects/pdb2pqr/</a>
APBS	<a href="#">[46]</a>	<a href="https://sourceforge.net/projects/apbs/files/apbs/">https://sourceforge.net/projects/apbs/files/apbs/</a>
QuikChange Primer Design tool	Agilent Technologies, CA	<a href="https://www.genomics.agilent.com/primerDesignProgram.jsp">https://www.genomics.agilent.com/primerDesignProgram.jsp</a>
Other		
Transcriptome Assembly – <i>G. niloticus</i>	This Paper	<a href="https://efishgenomics.integrativebiology.msu.edu">https://efishgenomics.integrativebiology.msu.edu</a>
Transcriptome Assembly – <i>P. soudanensis</i>	This Paper	<a href="https://efishgenomics.integrativebiology.msu.edu">https://efishgenomics.integrativebiology.msu.edu</a>

## CONTACT FOR REAGENT AND RESOURCE SHARING

Further information and requests for resources and reagents should be directed to and will be fulfilled by the Lead Contact, Harold H. Zakon ([h.zakon@austin.utexas.edu](mailto:h.zakon@austin.utexas.edu)). All materials generated by this study are available by request or as Internet resources where described.

## EXPERIMENTAL MODEL AND SUBJECT DETAILS

### Animal Sources

#### ***Petrocephalus soudanensis* [Osteoglossiformes: Mormyridae]**

A freshwater mormyrid species native to central Africa was obtained through the aquarium trade. Sex of individual was not determined. Cornell Museum of Vertebrates (CUMV: 91327, Specimen # 5727; Identified by M.E. Arnegard). Tissues were collected in RNAlater prior to RNA-isolation.

#### ***Gymnarchus niloticus* [Osteoglossiformes: Gymnarchidae]**

A freshwater species native to central Africa, was obtained through the aquarium trade. Sex of individual was not determined. Tissues were collected in RNAlater prior to RNA-isolation. All procedures used followed the American Physiological Society Animal Care Guidelines, and were approved by the Institutional Animal Care and Use Committee at University of Texas, Austin and Michigan State University.

### Oocytes

Mature 9+ cm Female, darkly pigmented *Xenopus laevis* were obtained from Nasco, WI (ITEM# LM00535MX) and housed in the University animal facility. Oocytes were surgically removed from the frogs in accordance with the NIH guidelines. The surgical procedure was done using tricane anesthesia under a protocol approved by the IACUC of the University of Texas at Austin. The surgically removed oocytes were placed in a solution containing 108 mM NaCl, 1 mM EDTA, 2 mM KCl, and 10 mM HEPES. The thecal and epithelial layers were manually removed from the oocytes. Oocytes were then treated for 10 minutes with 0.5 mg/mL collagenase from *Clostridium histolyticum* suspended in 83 mM NaCl, 2 mM KCl, 1 mM MgCl<sub>2</sub> and 5 mM HEPES to remove the follicular layer. De-folliculated Stage V and VI were used for all mRNA injections. mRNA microinjections were done using the micro injector from Drummond Scientific Co., PA. Injected oocytes were incubated at 16°C in sterile modified Barth's solution [88 mM NaCl, 1 mM KCl, 2.4 mM NaHCO<sub>3</sub>, 19 mM HEPES, 0.82 mM MgSO<sub>4</sub>, 0.33 mM Ca(NO<sub>3</sub>)<sub>2</sub>, 0.91 mM CaCl<sub>2</sub>, 10,000 units/l penicillin, 50 mg/l gentamicin, 90 mg/l theophylline, and 220 mg/l sodium pyruvate, pH 7.5] for 1–3 days after injection to achieve optimal channel expression for recordings.

## METHOD DETAILS

### RNA Extraction and Library Preparation for RNAseq

Tissues were homogenized in liquid nitrogen using a ceramic mortar and pestle, and total RNA was extracted using Trizol (ThermoFisher Scientific, Waltham, MA USA) following the manufacturer's specifications (see [42] for detailed methods). Total RNA was quantified using qubit and quality assessed using a Bioanalyzer (Agilent Technologies, Santa Clara, CA USA). Samples were then depleted of ribosomal RNA using the a RiboZero kit (Illumina, Inc. San Diego, CA) as per manufacturer's specifications, or RNA samples were again assessed for concentration and quality before preparation of sequencing libraries. cDNA libraries were constructed from ribosomal RNA-depleted samples using the Illumina TruSeq RNA Sample Preparation (v.2) kit. All libraries were sequenced on an Illumina HiSeq2500 using 125bp single-end reads (2x125bp). Various mRNA libraries were sequenced on various platforms as summarized in Table S1.

### Additional Data Sources

#### ***B. brachyistius***

We downloaded the raw reads for *Brienomyrus brachyistius* electric organ and skeletal muscle tissues referenced in [1] with NCBI BioProject: PRJNA248545.

#### ***C. compressirostris***

We downloaded the raw reads for skeletal muscle and electric organ tissue referenced in [47] with NCBI BioProject: PRJNA192446.

### Transcriptome Assembly

For each species, short read sequences obtained from each tissue were combined. Quality control, adapter trimming, and quality filtering was performed using Trimmomatic version 0.33 [39] with the following settings: ILLUMINACLIP TruSeq3-PE.fa:2:30:10 SLIDINGWINDOW:4:30 MINLEN:60. Paired trimmed reads for each species were then assembled into de-novo transcriptomes using Trinity v.20140413p1 [40] with default parameters. To speed up assembly, reads from *C. compressirostris* were digitally normalized prior to assembly using the `-normalize_reads` flag. Results of all assemblies are summarized in Table S2.

### Calculation of Expression Levels

Short reads from individual tissue libraries were mapped to the appropriate transcriptome assembly using Bowtie2 v. 2.2.6 [41] with default parameters. Read counting and ambiguity resolution were performed using RSEM v. 1.3.0, [42]. Raw read counts were then scaled and normalized per sample by transforming to FPKM values, and samples were cross-sample normalized using a trimmed mean of M values (TMM; [48]) for comparison between libraries and species. Scaling and normalization was performed using Trinity v.20140413p1 scripts 'align\_and\_estimate\_abundance.pl' and 'abundance\_estimates\_to\_matrix.pl' respectively.

### Assignment of Orthologues Between Electric Fish

Using SeaView (<http://doua.prabi.fr/software/seaview>) nucleotide or amino acid sequences of mormyrid potassium channel genes were aligned with potassium channel genes (in the shaker family: nucleotide = kcnax; amino acid = kv1.x) of other teleosts, and human. Trees were rooted with *D. melanogaster* shaker, the canonical shaker family channel. Alignments were analyzed in a maximum likelihood format using the default parameters (model of evolution = GTR; nucleotide equilibrium frequency = empirical; number of invariable sites = none; number of rate categories = four; 100 bootstrap replicates). We then utilized the branch-site random effects likelihood (REL) algorithm [49] (HYPHY website, <http://www.datamonkey.org/>) to identify branches that have undergone episodic diversifying selection. *B. brachyistius* kcna7a was the reference gene with 1545 nucleotides. For analysis of positive selection the N and C termini and a poorly aligned segment were trimmed so that the dataset for was nucleotides 172-678 and 748-1401. Different datasets included: kcna7a alone, kcna7a and kcna7b together, and both of these datasets with human kcna7 as outgroup. In all analyses, the same three branches (Figure 3 in red) were significant for evidence of positive selection.

### Mutagenesis and Expression in Oocytes

The coding sequences of Kcna7a genes from *Brienomyrus brachyistius* and *Gymnarchus niloticus* were synthesized by GenScript (Piscataway, NJ, USA) and cloned into the pGEMHE vector. During synthesis the Kozak sequence (GCCACC) was added to the 5' end of the sequences immediately before the start codon to improve translation efficiency. Mutations were introduced using the QuikChange II XL site directed mutagenesis kit from Agilent technologies, USA, and verified by sequencing. In-vitro transcription was carried out using the mMACHINE T7 transcription kit from Thermo Fisher Scientific as per the manufacturer's protocol. The concentration of the synthesized capped mRNA was measured using the ND-1000 spectrophotometer from NanoDrop Technologies, Wilmington, DE, USA. Each oocyte was injected with 50 nl of 0.01-0.1  $\mu\text{g}/\mu\text{l}$  mRNA suspended in nuclease free water.

### Electrophysiology and Analysis

Currents from mRNA injected oocytes was recorded using the two-electrode voltage clamp. All recordings were done at room temperature (21-23°C) using the OocyteClamp OC 725C amplifier from Warner Instruments Corp (Hamden, CT, USA). The bath solution contained 115 mM NaCl, 1.5 mM KCl, 10 mM HEPES and 1 mM MgCl<sub>2</sub>, pH- 7.4 adjusted with NaOH. The pipette solution consisted of 3 M KOAc and 15 mM KCl. Current activation was measured using a series of 10 mV voltage steps (100 ms each) from a potential of -90 mV to 40 mV followed by a 100 ms tail pulse of -50 mV. For recording currents from *Brienomyrus* mutants that open at more depolarized potentials the voltage steps used were -70 to 60 mV or 80 mV in 10 mV increments. The K<sup>+</sup> reversal potential was measured by a pulse protocol of 100 ms depolarization to 40 or 60 mV followed by a 200 ms test pulse of -120 mV to 0 mV in 10 mV increments. In all recordings the holding potential was maintained at -90 mV.

Data acquisition and the preliminary minimal analysis of I-V data were done using the pCLAMP 8 software from Axon Instruments, Inc., (Foster City, CA, USA). All other analysis was done using the GraphPad Prism 5 software. The ionic current (I) recorded during the voltage steps was converted to conductance (G) by dividing with the driving force (V-E<sub>rev</sub>). The half-activation potential (V<sub>1/2</sub>) and slope factor of the activation curve were obtained by fitting the G-V curves with a simple Boltzmann function. For calculation of tau-activation, the rising phase of the K<sup>+</sup> channel current at each voltage step was fitted with the equation I(t) = I<sub>max</sub>\*(1-exp(-K\*t))^n where K = 1/tau-activation. Although, we tried fitting with n = 2,3,4, the best overall fit was obtained with n = 2 and this has been used throughout this study. Time constants for deactivation were obtained by fitting with a single exponential.

### Computational Methods and Results

For numerical simulations we modeled the electrocyte as a single compartment. The capacitance C was 50 nF consistent with empirical measurements of whole-cell capacitance in electrocytes of weakly electric fish [50–52]. Differential equations were coded and integrated with Matlab (Mathworks, Inc., Natick MA) using Euler's method with integration time steps of 1 x 10<sup>-9</sup> sec. The current balance equation was:

$$C_m \frac{dV}{dt} = I_{stim}(t) - I_{Na} - I_K - I_R - I_L \quad (1)$$

where I<sub>Na</sub> represents Na<sup>+</sup> current, I<sub>K</sub> represents a non-inactivating delayed rectifier K<sup>+</sup> current, I<sub>R</sub> is an inwardly-rectifying K<sup>+</sup> current, and I<sub>L</sub> is the leak current. Equations for these currents were as follows:

$$I_{Na} = \bar{g}_{Na} m^3 h (V_m - 50) \quad (2)$$

$$I_K = \bar{g}_K n^4 (V_m + 105) \quad (3)$$

$$I_R = \bar{g}_R \left( \frac{1}{1 + \exp(\eta_R(V_m + 90))} \right) (V + 105) \quad (4)$$

$$I_L = \bar{g}_L (V_m + 95) \quad (5)$$

The gating variables in Equations 2 and 3 are given by Equation 6 where  $j = m, h,$  or  $n$ :

$$\frac{dj}{dt} = \frac{j_\infty(V_m) - j}{\tau_j(V_m)} \quad (6)$$

The voltage-dependent values of  $j_\infty$  evolved as follows:

$$j_\infty = \frac{1}{1 + \exp\left(\frac{V50_j - V_m}{k_j}\right)} \quad (7)$$

where  $V50_j$  and  $k_j$  are derived from Boltzmann sigmoidal fits to empirical from the present results for  $j = n$  and from previous empirical data for electrocyte  $\text{Na}^+$  conductances for  $j = m$  [51]. These values are given in Table S3.  $\tau_\phi$  is given by Eqn. 8 for  $j = m$  and  $n$ :

$$\tau_j = \frac{\alpha_j}{1 + \left(\frac{V_m - \mu_j}{\sigma_j}\right)^2} + \beta_j \quad (8)$$

and by Eqn. 9 for  $j = h$ :

$$\tau_j = \alpha_j \times \exp\left(-0.5 \times \left(\frac{V_m - \mu_j}{\sigma_j}\right)^2\right) + \beta_j \quad (9)$$

Where values of  $\alpha_j, \beta_j, \mu_j,$  and  $\sigma_j$  were determined by least-squares best fits to empirical data from the present results for  $j = n$ , and from previous empirical data [51] for  $j = m$  or  $h$ . These parameter values are given in Table S3.

We first compared simulated APs from model cells with identical  $\text{Na}^+$  and leak conductance parameters, but  $\text{K}^+$  conductance parameters derived from G-V and  $\tau$ -V curves for *kcna7a* of either *Gymnarchus* or *Brienomyrus* (Figure S2). To further explore the contributions of these parameters to changes in AP width, we then tested a set of 11305 model cells where we systematically varied  $k_n, V50_n,$  and  $\mu_n$  between the values for *Gymnarchus* and those for *Brienomyrus*, thereby changing the G-V curve slope, G-V curve midpoint, and  $\tau$ -V curve midpoint, respectively (parameter ranges are shown in Table S4). We then used stepwise multiple linear regression (Matlab *stepwiselm* function) to determine the relative contributions of these parameters in determining AP width across all combinations of these parameters.

### Structure Models

The Protein Modeling Portal, <https://www.proteinmodelportal.org> [43] was used to submit projects to multiple servers for structure prediction. *Kcna7a* voltage-sensor domain protein sequences were submitted using *Brienomyrus* (residues 276-340) and *Gymnarchus* (residues 275-337). Some solutions returned obvious steric clashes. As a final step, the Yasara server was used to energy minimize solutions, add hydrogens, and to alleviate steric clashes within the models (<http://www.yasara.org/minimizationserver.htm>) [44]. The values used for amino acid flexibility score were determined previously [53], and rendered in place of B-factors in the model output structure files. Electrostatic surface potential was determined using the PDB2PQR and APBS (Adaptive Poisson-Boltzmann Solver) plugins for The PyMOL Molecular Graphics System, Version 0.99rc6 (Schrödinger, LLC) [45, 46]).

## QUANTIFICATION AND STATISTICAL ANALYSIS

### Phylogenetic Analysis

Bootstrap values > 0.95 were considered significant support for nodes of phylogenetic trees. Assessment of episodic diversifying selection on nodes or branches of trees was done within the HyPhy format using the branch-site REL program. This uses the likelihood ratio test with a corrected p value of >0.01.

### Electrophysiology

Statistical analysis of electrophysiological results was performed using the GraphPad Prism 5 software. Statistical tests used were either Student's t test or one-way ANOVA followed by the Dunnett's post-test with a 95% confidence interval. For each experiment, the particular statistical tests used and significance thresholds are reported in each figure legend.

## DATA AND SOFTWARE AVAILABILITY

The raw sequence data generated in this project are available through the NCBI Sequence Read Archive (SRA) with the following BioProject accession numbers: SRP136188 and SRP136186. Assembled transcriptomes and expression tables are available for download and BLAST searching via the EFISHGENOMICS web-portal (<https://efishgenomics.integrativebiology.msu.edu>). Focal sequences described in this analysis have been additionally deposited in NCBI Genbank with the accession numbers described in [Table S5](#).